The supplementary data for the paper "Multiphase timing of hominin occupations and the paleoenvironment in Luonan Basin, Central China"

Huayu Lu, Hongyan Zhang, Shejiang Wang, Xuefeng Sun, Richard Cosgrove, Jun Zhao, Donghuai Sun, Chunfa Zhao, Chen Shen, Ming Wei

(Eemail: huayulu@nju.edu.cn)

Part 1

The paleomagnetic analysis of the loess deposit at Luonan Basin

The paleomagentic samples from Shangbaichuan loess section were measured three times to provide greater accuracy to constrain the ages of the loess deposit. During the fieldwork of 2006, we only collected 10 oriented samples at a limited number of "control points". These samples were measured in paleomeagnetic laboratory 'Fort Hoofddijk' , Faculty of Earth Sciences, Utrecht University (The Netherlands) and the Institute of Earth Environment, Chinese Academy of Sciences. One important finding was the provisional identification of the Brunhes/Matuyama boundary in the lower part of the Shangbaichuan loess-palesol sequence. This preliminary result was published in 2007 (Lu et al. 2007). To more precisely define the boundary and confirm its presence further detailed sampling took place at the Shangbaichuan and Liuwan sections. More than 120 oriented samples at finely spaced intervals of 20 cm were obtained. These were measured in paleomagnetic laboratory at Lanzhou University, China, and are reported here for the first time.

All oriented samples were systemically stepwise demagnetized in order to obtain the natural remnant magnetization (NRM). A comparison of alternation demagnetization (AF) and thermo demagnetization (TH) on these samples (Fig. S1) were conducted and the results show that both of the two demagnetizations had completely removed the secondary magnetic remnants (Fig. 3). However, the thermo demagnetization is better, so it is employed in this investigation to establish the magnetostratigraphy.

The thermo demagnetization was undertaken at room temperature to 630°C or

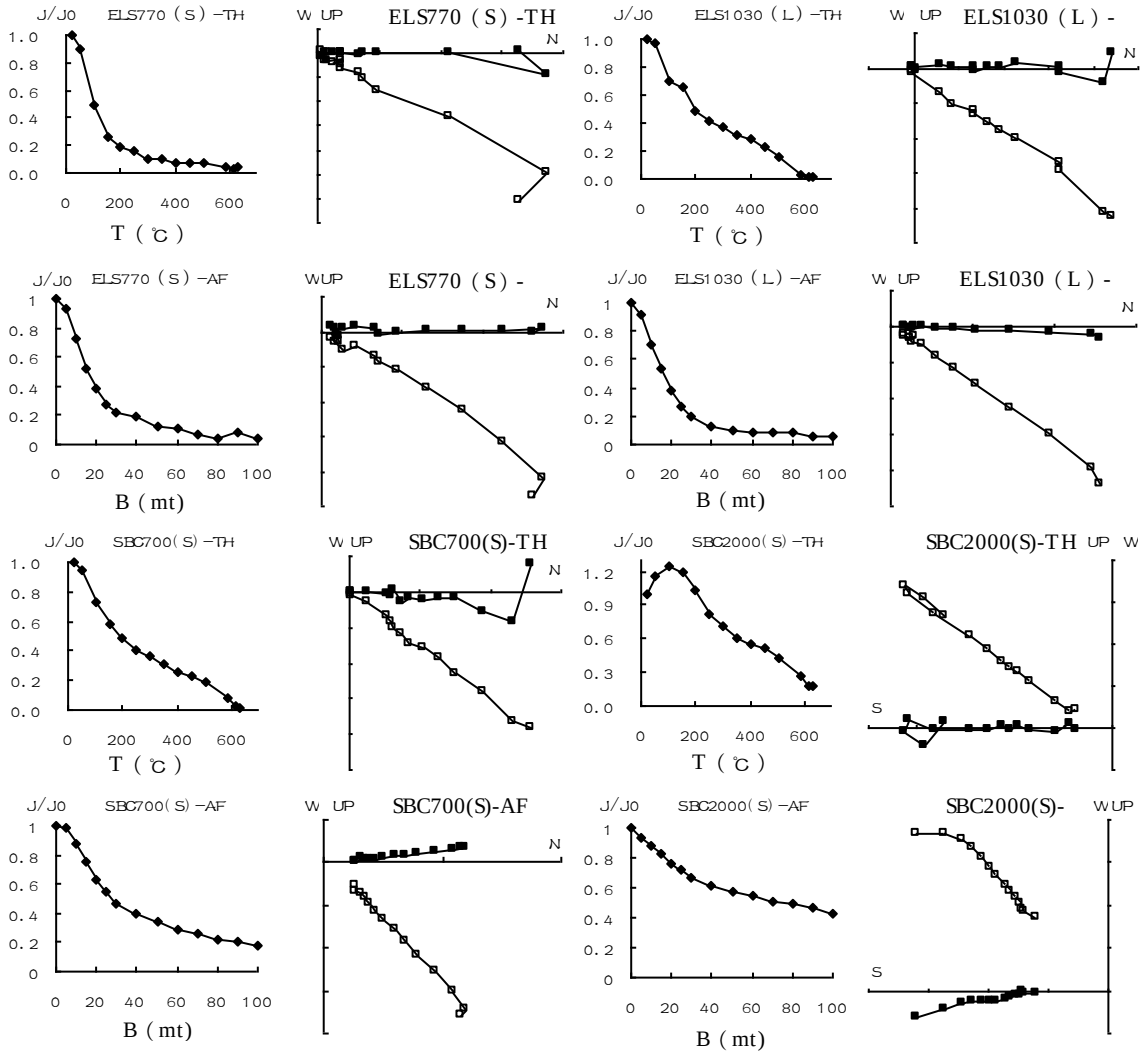

Fig. S1 A comparison of alternation demagnetization (AF) and thermo demagnetization (TH) on the loess samples.

Table S1 Original demagnetization data of the samples from Shangbaichuan and Liuwan sections

Sample II	Temp C	De:Unrotate	In: Unrotatec	Intensity	X corr	Y corr	Z corr		X drift	Y drift	Z drift	X bkg #1	X bkg #2	Y bkg #1	Y bkg #2	Z bkg #1	Z bkg #2	Treatment	Sample Timestamp
22	25	28.42	61.78	2.55E-04	1.06E-04	5.73E-05	2.24E-04	1.00	4.60E-10	1.92E-08	-5.73E-09	0.00E+00	6.92E-10	0.00E+00	2.88E-08	0.00E+00	-8.62E-09	Thermal	09/14/07 1611
22	50	35.49	55.92	2.55E-04	1.16E-04	8.28E-05	2.11E-04	1.00	0.00E+00	1.20E-08	-7.28E-09	0.00E+00	0.00E+00	0.00E+00	1.82E-08	0.00E+00	-1.10E-08	Thermal	09/14/07 1836
22	100	15.83	53.13	2.08E-04	1.20E-04	3.40E-05	1.66E-04	0.82	-4.59E-10	8.02E-09	-4.48E-09	0.00E+00	-6.92E-10	0.00E+00	1.21E-08	0.00E+00	-6.76E-09	Thermal	09/14/07 2004
22	150	14.55	51.47	1.55E-04	9.32E-05	2.42E-05	1.21E-04	0.61	6.89E-10	8.98E-09	-7.29E-09	0.00E+00	1.04E-09	0.00E+00	1.35E-08	0.00E+00	-1.10E-08	Thermal	09/14/07 2215
22	200	17.54	49.38	1.13E-04	7.02E-05	2.22E-05	8.59E-05	0.44	2.29E-10	9.17E-09	-3.24E-09	0.00E+00	3.46E-10	0.00E+00	1.39E-08	0.00E+00	-4.90E-09	Thermal	09/15/07 1230
22	250	20.23	52.19	8.37E-05	4.82E-05	1.78E-05	6.61E-05	0.33	-1.37E-09	1.53E-08	-2.24E-09	0.00E+00	-2.08E-09	0.00E+00	2.31E-08	0.00E+00	-3.38E-09	Thermal	09/15/07 2143
22	300	19.03	48.57	6.64E-05	4.15E-05	1.43E-05	4.98E-05	0.26	2.07E-09	1.14E-08	-3.37E-10	0.00E+00	3.11E-09	0.00E+00	1.71E-08	0.00E+00	-5.07E-10	Thermal	09/15/07 1248
22	350	20.58	49.64	5.47E-05	3.31E-05	1.24E-05	4.17E-05	0.21	1.61E-09	1.23E-08	-7.84E-09	0.00E+00	2.42E-09	0.00E+00	1.85E-08	0.00E+00	-1.18E-08	Thermal	09/15/07 1506
22	400	18.39	48.97	4.68E-05	2.92E-05	9.69E-06	3.53E-05	0.18	-6.90E-10	1.09E-08	-1.91E-09	0.00E+00	-1.04E-09	0.00E+00	1.64E-08	0.00E+00	-2.87E-09	Thermal	09/15/07 1713
22	450	14.1	48.35	3.78E-05	2.43E-05	6.11E-06	2.82E-05	0.15	3.21E-09	1.63E-08	1.01E-08	0.00E+00	4.84E-09	0.00E+00	2.46E-08	0.00E+00	1.52E-08	Thermal	09/15/07 1932
22	500	20.81	54.44	2.77E-05	1.51E-05	5.73E-06	2.26E-05	0.11	1.37E-09	5.18E-09	2.91E-09	0.00E+00	2.08E-09	0.00E+00	7.83E-09	0.00E+00	4.39E-09	Thermal	09/15/07 2149
22	525	20.62	47.28	2.32E-05	1.48E-05	5.55E-06	1.71E-05	0.09	3.66E-09	1.27E-08	2.23E-09	0.00E+00	5.54E-09	0.00E+00	1.92E-08	0.00E+00	3.38E-09	Thermal	09/16/07 1239
22	550	19.97	47.03	2.22E-05	1.42E-05	5.18E-06	1.63E-05	0.09	-2.98E-09	1.25E-08	3.13E-09	0.00E+00	-4.50E-09	0.00E+00	1.89E-08	0.00E+00	4.73E-09	Thermal	09/16/07 2135
22	580	12.07	49.6	1.06E-05	6.70E-06	1.43E-06	8.05E-06	0.04	-2.98E-09	9.21E-09	6.17E-09	0.00E+00	-4.50E-09	0.00E+00	1.39E-08	0.00E+00	9.30E-09	Thermal	09/16/07 1236
22	610	345.84	44.3	5.21E-06	3.62E-06	-9.12E-07	3.64E-06	0.02	-1.88E-08	1.80E-08	1.01E-09	0.00E+00	-2.84E-08	0.00E+00	2.71E-08	0.00E+00	1.52E-09	Thermal	09/16/07 1518
22	650	11.55	-2.83	2.62E-06	2.56E-06	5.23E-07	-1.29E-07	0.01	-3.91E-09	1.16E-08	-8.98E-10	0.00E+00	-5.88E-09	0.00E+00	1.74E-08	0.00E+00	-1.35E-09	Thermal	09/16/07 1821

Sample ID	Temp C	De:Unrotat	In: Unrotat	Intensity	X corr	Y corr	Z corr		X drift	Y drift	Z drift	X bkg #1	X bkg #2	Y bkg #1	Y bkg #2	Z bkg #1	Z bkg #2	Treatment	Sample Timestamp
29	25	351.52	49.78	1.32E-04	8.43E-05	-1.26E-05	1.01E-04	1.00	-9.86E-09	1.07E-08	-7.55E-09	0.00E+00	-1.76E-08	0.00E+00	1.92E-08	0.00E+00	-1.35E-08	Thermal	09/14/07 1621
29	50	356.55	50.38	1.40E-04	8.92E-05	-5.38E-06	1.08E-04	1.06	2.12E-09	7.14E-09	-1.69E-09	0.00E+00	3.81E-09	0.00E+00	1.28E-08	0.00E+00	-3.04E-09	Thermal	09/14/07 1841
29	100	355.45	51.06	1.19E-04	7.47E-05	-5.94E-06	9.28E-05	0.90	9.71E-10	7.19E-09	-4.74E-10	0.00E+00	1.73E-09	0.00E+00	1.28E-08	0.00E+00	-8.45E-10	Thermal	09/14/07 2012
29	150	357.99	50.58	1.04E-04	6.58E-05	-2.31E-06	8.01E-05	0.79	1.92E-10	6.73E-09	-3.20E-09	0.00E+00	3.46E-10	0.00E+00	1.21E-08	0.00E+00	-5.75E-09	Thermal	09/14/07 2220
29	200	356.99	51.24	9.17E-05	5.73E-05	-3.02E-06	7.15E-05	0.69	9.61E-10	8.71E-09	3.19E-09	0.00E+00	1.73E-09	0.00E+00	1.57E-08	0.00E+00	5.75E-09	Thermal	09/15/07 1238
29	250	355.25	50.58	6.99E-05	4.42E-05	-3.68E-06	5.40E-05	0.53	-3.85E-10	1.15E-08	-3.29E-09	0.00E+00	-6.92E-10	0.00E+00	2.06E-08	0.00E+00	-5.92E-09	Thermal	09/15/07 2148
29	300	358.06	50.44	5.71E-05	3.63E-05	-1.23E-06	4.40E-05	0.43	3.85E-10	1.17E-08	-4.32E-09	0.00E+00	6.92E-10	0.00E+00	2.10E-08	0.00E+00	-7.77E-09	Thermal	09/15/07 1254
29	350	354.92	49.29	4.87E-05	3.16E-05	-2.81E-06	3.69E-05	0.37	2.51E-09	9.33E-09	-1.60E-09	0.00E+00	4.50E-09	0.00E+00	1.67E-08	0.00E+00	-2.87E-09	Thermal	09/15/07 1511
29	400	351.82	50.21	4.19E-05	2.65E-05	-3.81E-06	3.22E-05	0.32	9.60E-10	7.11E-09	6.57E-10	0.00E+00	1.73E-09	0.00E+00	1.28E-08	0.00E+00	1.18E-09	Thermal	09/15/07 1718
29	450	352.08	51.41	3.53E-05	2.18E-05	-3.03E-06	2.76E-05	0.27	1.34E-09	1.05E-08	2.90E-09	0.00E+00	2.42E-09	0.00E+00	1.89E-08	0.00E+00	5.24E-09	Thermal	09/15/07 1938
29	500	0.57	50.23	2.63E-05	1.68E-05	1.66E-07	2.02E-05	0.20	3.10E-09	8.58E-09	-2.84E-09	0.00E+00	5.54E-09	0.00E+00	1.53E-08	0.00E+00	-5.07E-09	Thermal	09/15/07 2155
29	525	353.47	49.72	2.27E-05	1.46E-05	-1.67E-06	1.73E-05	0.17	2.30E-09	6.90E-09	4.68E-10	0.00E+00	4.15E-09	0.00E+00	1.25E-08	0.00E+00	8.45E-10	Thermal	09/16/07 1244
29	550	355.2	48.17	2.10E-05	1.39E-05	-1.17E-06	1.56E-05	0.16	-3.45E-09	1.10E-08	4.58E-09	0.00E+00	-6.23E-09	0.00E+00	1.99E-08	0.00E+00	8.28E-09	Thermal	09/16/07 2139
29	580	354.61	41.89	1.12E-05	8.32E-06	-7.84E-07	7.49E-06	0.09	-2.48E-09	9.61E-09	5.12E-09	0.00E+00	-4.50E-09	0.00E+00	1.74E-08	0.00E+00	9.30E-09	Thermal	09/16/07 1240
29	610	356.89	45.03	7.13E-06	5.03E-06	-2.73E-07	5.04E-06	0.05	-7.63E-09	1.39E-08	3.17E-09	0.00E+00	-1.38E-08	0.00E+00	2.53E-08	0.00E+00	5.75E-09	Thermal	09/16/07 1522
29	650	349.13	49.39	5.64E-06	3.60E-06	-6.92E-07	4.28E-06	0.04	-9.55E-10	1.06E-08	-1.31E-09	0.00E+00	-1.73E-09	0.00E+00	1.92E-08	0.00E+00	-2.37E-09	Thermal	09/16/07 1825

Demag(°C)	X	Y	Z	Intensity	J/Jmax			Year	
25	6.93E-05	-8.95E-06	1.21E-04	0.0001399	1.00	Apr	12	2007	20:30
50	7.12E-05	1.87E-05	1.24E-04	0.0001443	1.03	Apr	13	2007	15:10
100	6.15E-05	1.60E-05	1.14E-04	0.0001303	0.93	Apr	14	2007	17:34
150	5.07E-05	1.28E-05	8.99E-05	0.000104	0.74	Apr	15	2007	10:52
200	4.01E-05	8.85E-06	7.75E-05	8.774E-05	0.63	Apr	16	2007	12:34
250	3.15E-05	1.08E-05	5.78E-05	6.667E-05	0.48	Apr	16	2007	20:25
300	2.64E-05	6.89E-06	4.73E-05	5.465E-05	0.39	Apr	17	2007	18:57
350	2.51E-05	-2.34E-06	4.62E-05	5.267E-05	0.38	Apr	18	2007	10:36
400	2.26E-05	5.13E-06	3.62E-05	4.299E-05	0.31	Apr	18	2007	20:28
450	1.90E-05	5.10E-06	3.23E-05	3.779E-05	0.27	Apr	19	2007	18:11
500	1.75E-05	1.61E-06	2.72E-05	3.236E-05	0.23	Apr	19	2007	23:38
580	7.98E-06	-6.35E-07	1.56E-05	1.751E-05	0.13	Apr	20	2007	18:46
610	5.69E-06	2.05E-06	9.06E-06	1.09E-05	0.08	Apr	21	2007	1:03
630	4.77E-06	2.47E-06	7.95E-06	9.593E-06	0.07	Apr	21	2007	20:31

Demag(°C)	X	Y	Z	Intensity	J/Jmax			Year	
25	-1.30E-05	4.00E-06	-3.38E-05	3.64224E-05	1.00	Apr	12	2007	22:27
50	-2.79E-05	-6.91E-06	-4.65E-05	5.46409E-05	1.50	Apr	13	2007	21:06
100	-3.29E-05	-1.11E-05	-5.37E-05	6.39103E-05	1.75	Apr	14	2007	20:16
150	-3.63E-05	-7.37E-06	-5.10E-05	6.29966E-05	1.73	Apr	16	2007	10:53
200	-3.49E-05	-6.30E-06	-4.75E-05	5.92288E-05	1.63	Apr	16	2007	18:02
250	-2.75E-05	-4.78E-06	-3.71E-05	4.6393E-05	1.27	Apr	17	2007	10:50
300	-2.42E-05	-4.44E-06	-3.21E-05	4.04147E-05	1.11	Apr	17	2007	21:00
350	-1.92E-05	-5.49E-06	-2.69E-05	3.35417E-05	0.92	Apr	18	2007	18:27
400	-1.79E-05	-3.34E-06	-2.34E-05	2.96538E-05	0.81	Apr	19	2007	10:26
450	-1.46E-05	-3.99E-06	-2.08E-05	2.57383E-05	0.71	Apr	19	2007	21:22
500	-1.26E-05	-1.95E-06	-1.69E-05	2.11824E-05	0.58	Apr	20	2007	11:21
580	-7.45E-06	-2.29E-06	-8.37E-06	1.1435E-05	0.31	Apr	20	2007	21:47
610	-4.81E-07	-2.50E-06	-6.40E-06	6.89033E-06	0.19	Apr	21	2007	3:52
630	-2.75E-06	1.04E-06	-3.24E-06	4.3732E-06	0.12	Apr	21	2007	22:57

650°C at intervals of 25-50°C in the zero magnetic fields; the progressive demagnetization successfully isolated the characteristic remnant magnetization (ChRM) components after removing a viscous component of magnetization subsequent to the 150-300°C treatment (Please see the supplementary data for *The demagnetization LW140; The demagnetization LW990; The demagnetization sbc560; The demagnetization sbc2260*; for examples). A 2G-760R superconductor magnetic meter measured the demagnetized samples and the principal components analysis was computed by a ‘‘least-squares fit’’ technique (Kirschvink, 1980). On the basis of this method, the inclination and declination of each oriented samples was obtained and the magnetostratigraphy of each loess-paleosol sequence is presented in Fig. 4.

References

Kirschvink, J. L., 1980. The least-square line and plane and the analysis of paleomagnetic data. Geophysical Journal of the Royal Astronomical Society 62, 699-718.

Part 2

The Optically Stimulated Luminescence (OSL) dating of the loess deposit. (Originally reported in Lu et al. 2007). Additional information is shown in Table S2. Methods supplied by Dr Thomas Stevens, Oxford University).

Iron tubes (~25 cm long, ~8 cm diameter) were hammered into the cleaned section to obtain OSL dating samples. Samples were wrapped in light-tight black plastic bags immediately after extraction from the sections and were processed in the Oxford University Luminescence Dating Laboratory under subdued red light. Sunlight-exposed ends of samples were excluded from equivalent dose (De) determinations but retained for radioisotope measurements (to determine dose rate). Carbonates and organic matter were removed from the De (unexposed) fractions using 0.1 M HCl and 15% H_2O_2. Quartz was isolated by immersion in 35% H_2SiF_6 for up to 4 weeks with a subsequent 0.1 M HCl wash to remove fluorite precipitates. The coarse silt fraction (40-63 μm) was obtained by wet sieving. Prior to analysis, feldspar contamination was assessed by applying an IR depletion ratio test to 3-5 aliquots of each sample following the procedure of (Duller, 2003). Ratios of the two test dose

corrected 20 Gy OSL signals, one following a 60 s of IR diode stimulation at 40º C, were examined and any samples showing aliquots with ratios >10% away from unity were placed in H_2SiF_6 for a further 2 weeks. In all cases this resulted in samples passing the IR test.

De values were measured using a modified SAR procedure (Murray and Wintle, 2000) performed on a Risø TL-DA-15 TL/OSL reader. A blue LED (λ = ~470 nm) stimulation source was used (60 s, c. 400 mJ.cm-1) on samples and the OSL signal was measured using a 9235QA photomultiplier tube filtered by 6 mm of Hoya U340 (Bøtter-Jensen et al., 2000). Prior to blue LED OSL signal measurement, an elevated temperature IR signal was obtained from samples (Bailey and Arnold, 2006). This involved an initial 50 s stimulation at 160º C using IR diodes (λ = ~830 nm) at 90% power, followed by a second heating to 160º C for 240 seconds. During this second heating, IR diodes were switched on between 40 and 200 s.

Equivalent doses presented here were calculated using the blue stimulated OSL signal, integrated from the first 0.6 s of stimulation minus a background estimated from the last 6 s of stimulation. All growth curves were fitted using a saturating exponential plus linear function. Aliquots yielding recycling ratios (Murray and Wintle, 2000) differing from unity by greater than 10% were rejected. The uncertainty on individual De values was estimated using Monte Carlo simulation and a weighted mean De (with one standard error uncertainty) was calculated for each sample (typically ~14 aliquots). Application of elevated temperature IR stimulation to quartz grains enables sampling of the thermally stable OSL fast component with considerably less than 1% signal loss (Bailey and Arnold, 2006). The procedure also has the benefit of eliminating any low temperature (40º C) IR signal not detected in the OSL IR depletion ratio test (Duller, 2003), as in the 'post-IR OSL' investigations on polyminerals of Stokes et al. (2003), Roberts and Wintle (2003) and Wang et al. (2006), but will not affect equivalent doses from blue light stimulated OSL measurements presented here.

Dose rates were calculated from uranium, thorium and potassium contents measured using Inductively Coupled Plasma Mass Spectrometry (ICP-MS). ICP samples were prepared by sodium peroxide fusion. Dose rates were calculated using an alpha efficiency of 0.04 ± 0.02 (Rees-Jones, 1995) and sample-specific water contents determined through laboratory analysis (Table S2). Alpha and beta

attenuation was calculated using calculations in Bell (1980) and Mejdahl (1979) respectively and dose rate conversion factors were taken from Adamiec and Aitken (1998). Uncertainties are based on the propagation, in quadrature, of individual errors for all measured quantities, which if unknown are taken as 10%. In addition to uncertainties calculated from counting statistics, errors due to 1) beta source calibration (3%) (Armitage and Bailey, 2005), 2) radioisotope concentration (Table S2), 3) dose rate conversion factors (3%) and 4) attenuation factors (3%) have been included (Murray and Olley, 2002). The cosmic dose was calculated using present day burial depth (Prescott and Hutton, 1994). De, dosimetry and age data are presented in Table S2. Comparison of equivalent doses obtained using different OSL signal integration limits (0-0.12, 0-0.3. 0-0.6, 0-1.2, 0-1.8, 0-2.4 s) showed that all yielded results identical within error acceptable margins. Although the ages obtained are considerably older, the growth curves for the samples show that saturation has not yet been reached. As such the dates are considered accurate, although to be conservative, they are quoted to 2 σ in Table S2.

References

Adamiec, G., and Aitken M.J., 1998. Dose rate conversion factors: update. Ancient TL 16, 37-50.

Armitage, S. J., and Bailey, R.M., 2005. The measured dependence of laboratory beta dose rates on sample grain size. Radiation Measurements 39, 123-127.

Bailey, R. M. and Arnold, L. J., 2006. Statistical modelling of single grain quartz De distributions and an assessment of procedures for estimating burial dose. Quaternary Science Reviews 25, 2475-2502.

Bell, W. T., 1980. Alpha dose attenuation in quartz grains for thermoluminescence dating. Ancient TL 12, 4-8.

Bøtter-Jensen, L., Bulur, E., Duller, G. A. T., and Murray, A. S., 2000. Advances in luminescence instrumentation. Radiation Measurements 32, 523-528.

Duller, G. A. T., 2003. Distinguishing quartz and feldspar in single grain luminescence measurements. Radiation Measurements 37, 161-165.

Mejdahl, V., 1979. Thermoluminescence dating: beta-dose attenuation in quartz grains. Archaeometry 21, 61-72.

Murray, A. S., and Olley, J. M., 2002. Precision and accuracy in the optically stimulated luminescence dating of sedimentary quartz: A status review.

Geochronometria 21, 1-16.

Murray, A. S., and Wintle, A. G., 2000. Luminescence dating of quartz using an improved single-aliquot regenerative-dose procedure. Radiation Measurements, 32, 57-73.

Prescott, J. R., and Hutton J. T., 1994. Cosmic ray contributions to dose rates for luminescence and ESR dating: large depths and long term variations. Radiation Measurements 23, 497-500.

Rees- Jones, J., 1995. Optical dating of young sediments using fine-grain quartz: Ancient TL 13, 9-13.

Roberts, H. M., and Wintle, A. G., 2003. Luminescence sensitivity changes of polymineral fine grains during IRSL and [post-IR] OSL measurements. Radiation Measurements 37, 661-671.

Stevens, T., Armitage, S.J., Lu, H. Y., and Thomas D.S.G., 2007. Examining the potential of high sampling resolution OSL dating of Chinese loess: Quaternary Geochronology 2, 15-22.

Stokes, S., Hetzel, R., Bailey, R.M., Mingxin, T., 2003. Combined IRSL-OSL single aliquot regeneration (SAR) equivalent dose (De) estimates from source proximal Chinese loess. Quaternary Science Reviews 22, 975-983.

Wang, X., Lu, Y., Zhao, H., 2006. On the performances of single-aliquot regenerative-dose (SAR) protocol for Chinese loess: fine quartz and polymineral grains. Radiation Measurements 41, 1-8.

Table S2 The OSL sample data from upper part of the Shangbaichuan and Liuwan loess-paleosol sequences, the age results have been reported previously in the 2007 Chinese paper (Lu et al., 2007) .

Sample	Depth (cm)	U (ppm)	Th (ppm)	K (%)	Cosmic (Gy/ka)	Water C. (%)	Dose rate (Gy/ka)	De (Gy)	n	Age (ka)
SBC										
A	80	2.67±0.09	11.9±0.4	2.18±0.01	0.20±0.01	13.8±0.1	3.64±0.11	517.8±19.3	14	144.7 ± 7.4
B	140	2.93±0.10	14.6±0.5	2.03±0.01	0.19±0.01	16.8±0.2	3.65±0.12	707.0± 9.2	13	191.3 ± 7.5
C	320	2.65±0.09	11.0±0.3	2.02±0.01	0.15±0.01	17.7±0.2	3.25±0.10	741.9±11.8	14	223.6 ± 8.7
D	420	2.49±0.09	8.4±0.3	1.79±0.01	0.13±0.01	13.6±0.1	2.93±0.09	1033.7±19.6	14	359.3 ± 14.4
LW										
E	90	2.67±0.09	11.5±0.4	2.11±0.01	0.20±0.01	18.7±0.2	3.38±0.10	495.3±38.9	13	146.4 ± 12.3
F	160	2.76±0.10	11.8±0.4	2.16±0.01	0.18±0.01	19.9±0.2	3.41±0.10	472.3±44.0	14	137.0 ± 13.4
G	220	2.65±0.09	11.5±0.4	2.09±0.01	0.17±0.01	17.9±0.2	3.35±0.10	504.7± 5.1	14	151.6 ± 4.9
H	340	2.61±0.09	10.6±0.3	2.09±0.01	0.14±0.01	18.0±0.2	3.24±0.10	652.0±10.1	14	202.2 ± 6.9

Part 3

The pedostratigraphy of Shangbaichuan loess-paleosol section

1 Pedostratigraphy of Shangbaichuan loess-paleosol section (Table S3)

Table S3 Description of the Shangbaichuan (SBC) loess-paleosol sequence

Unit	Name	Depth/m	Color	Characters
1	paleosol	0-1.9	dark reddish-brown (2.5YR 5/4) to light reddish-brown (5YR 5/6), mottled	There are plant roots from surface to depth of 2 m. The particles are fine; it has a block structure with perpendicular crannies; there are black films of manganese oxide
2	loess	1.9-2.6	light brown (7.5YR 5/8), mottled with black spots	There are soil agglomerates and light coloured sand-silt blocks, and imprints of insects and plants
3	paleosol	2.6-3.6	dark reddish brown (5YR 3/6)	Clay with tiny holes and black film of manganese oxide, block structure with perpendicular crannies, imprints of insects and plants are weak
4	loess	3.6-4.6	light reddish-brown (10YR 6/8), mottled	Silt with more imprints of insects and plants, reddish films of ferric oxide and tiny holes
5	paleosol	4.6-6.4	light reddish (7.5YR 5/6)	There are tiny holes, black spots and imprints of insects, prism shaped blocks and films of manganese oxide and silt-clay deposit
6	loess	6.4-7.6	light red-brown (10YR 6/8), mottled	Block structure, silt with relatively denser imprints of insects; there are black spots and light olive-green silt-sandy agglomerates
7	paleosol	7.6-8.2	light brown (7.5YR 5/8)	Silt with more tiny holes and black spots of manganese oxide; perpendicular fissures are clear and prism shaped blocks are evident

8	paleosol	8.2-10.5	light brown (7.5YR 5/6) at lower part, and grey-yellow at upper part (2.5YR 6/2), in between are light-brown strips (7.5YR 5/8), mottled	Silt with black films of manganese oxide and red-brown ferric oxide, the films are denser in lower sections. There are imprints of insect activities, and bleaching; it is hard and there are perpendicular fissures
9	paleosol	10.5-11.5	dark red-brown (2.5YR 4/4)	Clay with silt agglomerates, perpendicular fissures are well developed; there are prism shaped blocks with a relatively more consistent colour in the lower part
10	loess	11.5-12.0	light brown (7.5YR 5/6)	Silt with brown-reddish silt agglomerates and black films of manganese oxide. Water seepage here and the underlying paleosol may serve as a barrier to block water from upper part
11	paleosol	12.0-12.8	red-brown (5YR 4/6)	Clay with perpendicular fissures and prism shaped block structure, and black films of manganese oxide
12	loess	12.8-15.0	light brown (7.5YR 5/6)	Silt, with tiny holes and biological imprints. There are dense films of manganese oxide; water is seeping out in the lower parts.
13	paleosol	15.0-15.7	light red-brown (7.5YR 5/8)	Fine particles with perpendicular fissures and prism shaped blocks. There are black films of manganese oxide and small silt agglomerates
14	loess	15.7-17.0	light red-brown (10YR 6/6), mottled	Silt, with tiny holes, biological activity and black films of manganese oxide
15	paleosol	17.0-17.8	red-brown (2.5YR 4/6)	Clay with perpendicular fissures and prism shaped blocks. There are pure black films of manganese and silt agglomerates and needle-shaped structures
16	loess	17.8-18.5	light red-brown (7.5YR 5/8)	Silt with a needle-shaped structure, there are black films of manganese and red-brown clay agglomerates
17	paleosol	18.5-19.7	red-brown (5YR 4/6)	Clay, hard, with perpendicular fissures, reddish ferric oxide and black films of manganese

18	loess	19.7-21.5	red-orange (7.5YR 6/6) at upper part and yellow to light yellow-red (2.5Y 6/6) at lower part, mottled	Silt with needle-shaped structures, with black spots of manganese and imprints of biological activities
19	paleosol	21.5-22.2	red-brown (5YR 4/4)	Hard clay, with dense films of manganese oxide and imprints of insect activities, and needle-shaped structures and silt particles
20	loess	22.2-23.3	light red-brown (10YR 6/8)	Silt with denser needle-shaped structures, black spots of manganese and a few imprints of insect activities, with pure light red-brown films of ferric oxide
21	paleosol	23.3-24.8	red-brown (5YR 4/8)	Clay with silt agglomerates, with a few needle-shaped holes, pure black films of manganese oxide and imprints of insect activities. There are separate spots of silver-color metal-oxide film

References

Shaanxi Provincial Institute of Archaeology, Cultural Relics Administrative Committee of ShangluoDistrict, Museum of Luonan County, 2007. Huashilang (I): The The Palaeolithic Open-air Sites in the Luonan Basin, China. Beijing, Science Press, pp.1-300.

Wang, S. J., Cosgrove, R., Lu, H. Y., Shen, C., Wei, M., Zhang, X. B., 2008. New progress on Paleolithic archaeological studies in the Luonan Basin, China. In: Matsufuji Kazuto ed. Loess-paleosol and Paleolithic chronology in East Asia. Tokyo, Yuzankaku, pp. 145-161.

2 Pedostratigraphy of Liuwan loess-paleosol section (Table S4)

Table S4 Description of the Liuwan loess-paleosol sequence

Unit	Name	Depth/m	Color	Characters
1	modern cultivated soil	0-0.5	yellow-brown (10YR 5/6)	Dense root mat and worm hole; loose with serious human disturbance; with broken tiles are found at depth of 0.4 m

2	loess	0.5-1.3	light brown (7.5YR 5/6)	Blocks of silts, with worm holes, plant roots etc, with clear perpendicular fissures; there are separate black-brown films of manganese and ferric oxides
3	paleosol	1.3-2.4	heavy red-brown (5YR 4/4)	Soil agglomerates with clay particles; black spots of manganese oxide and a few black carbon fragments
4	loess	2.4-2.8	light brown (7.5YR 5/6)	There are soil agglomerates, worm holes and imprints of plant roots; as well as spots of calcium carbonate with a diameter of circa 5 mm
5	paleosol	2.8-3.6	dark red-brown (5YR 4/4)	Soil agglomerates with a perpendicular structure and there are black spots of manganese oxide; olive-yellow agglomerates (5Y 6/4) which may be caused by bleaching
6	loess	3.6-4.0	light yellow-brown (10YR 6/6)	Silt and soil agglomerates, black spots of manganese oxide; olive-yellow (5Y 6/4) agglomerates may be caused by bleaching. There is surface erosion
7	paleosol	4.0-5.8	red-brown (5YR 4/6)	Soil agglomerates, with spots and films of black manganese oxide and imprints of biological activities; there are agglomerates of light yellow (5GY 8/3) in the lower part, which may be caused by bleaching. A small quartzite pebble is found at depth of 5.5 m.
8	loess	5.8-6.0	light yellow-brown (10YR 6/6)	Silt agglomerates with black spots and grey olive-yellow blocks occasionally with imprints of insect activities.
9	paleosol	6.0-7.0	dark red-brown (5YR 4/4), mottled with black and olive-yellow spots	Clay agglomerates with evidence of insect activity.
10	loess	7.0-7.4	light brown (7.5YR 5/6),	Silt with black spots

			mottled	
11	paleosol	7.4-8.2	Red-brown (5YR 4/6)	Clay, with black and ferrugineous spots and clusters, and insect imprints
12	loess	8.2-9.4	Light brown (7.5YR 5/6) , mottled	Silt, with spots and black ramiform films of manganese oxide, with olive-color agglomerates, becoming darker toward the lower levels
13	paleosol	9.4-9.9	red-brown (5YR 4/6)	Clayey, with black films of manganese oxides and olive-color agglomerates, as well as biological activity
14	loess	9.9-11.8	light brown (7.5YR 5/6), mottled.	Silt, with olive-colour agglomerates and biological imprints, with black films of manganese oxide
15	loess with fluvial sand and pebbles	11.8-12.5	light brown (7.5YR 5/6, mottled	Pebbles with diameter of 1-5 mm, with larger ones up to 2 cm; poorly sorted
16	fluvial sand and pebble	12.5-13.0	light brown (7.5YR 5/6)	Mixture of silt to pebble sized particles with the pebbles having a diameter of 1-2 cm. They are poorly sorted with some angularity. It is a fluvial-alluvial deposit without pedogenesis

Fig. S2 The Luonan Basin

Fig. S3 Photos of Shangbaichuan Loess-paleosol section

Fig. S4 Sampling Shangbaichuan Loess-paleosol section

Fig. S5 Sampling Shangbaichuan Loess-paleosol deposit from a well.

Fig. S6 Sampling the Liuwan Loess-paleosol section

Part 4

More specific information of the human fossil tooth from Luonan Basin (Fig. S7 and S8)

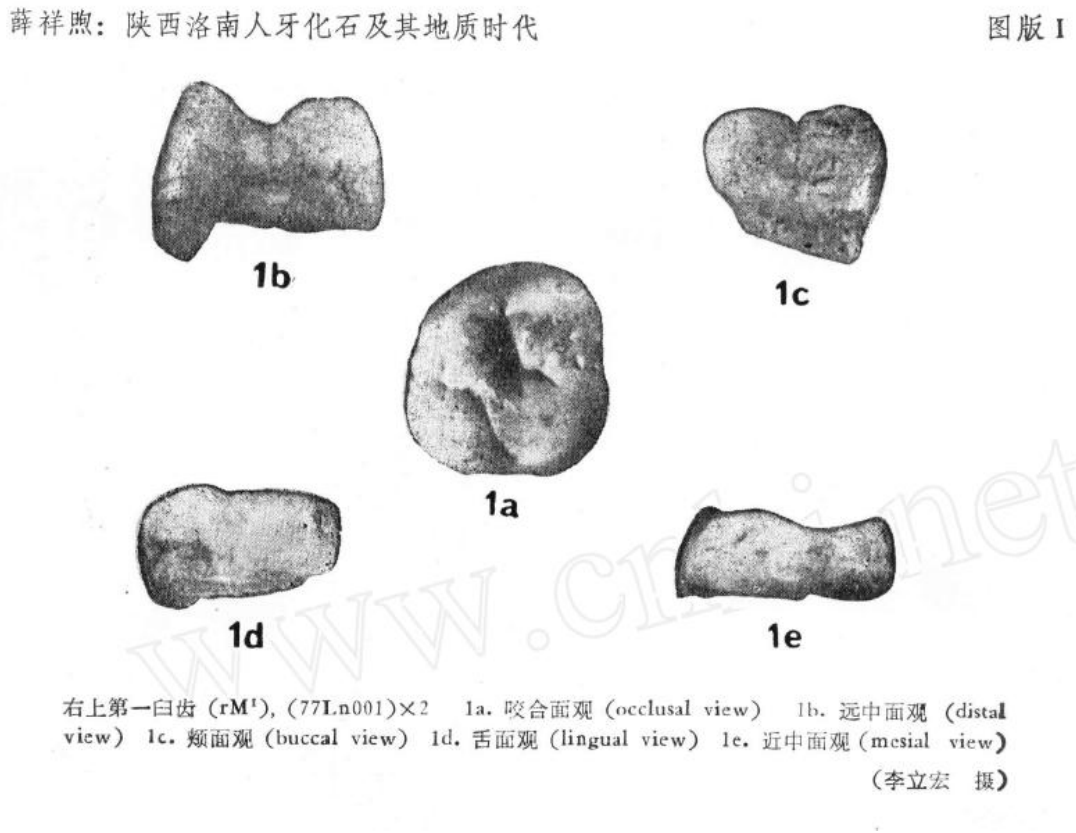

Fig. S7　Photos of the human fossil tooth found at Luonan Basin　(1a occlusal view; 1b distal view; 1c buccal view; 1d lingual view; 1e mesial view) (From Xue, 1987, Acta Anthropologica Sinica, 6(4): 284-288.)

HUMAN FOSSIL TOOTH FROM LUONAN, SHAANXI, AND ITS GEOLOGICAL AGE

Xue Xiangxu

(*Department of Geology, Northwest University, Xian*)

Key words Human fossil tooth; Luonan; Early Middle Pleistocene

Abstract

A right M^1 of human fossil, associated with a left M^1 of *Ailuropoda* and a right M^1 (or M^2) of *Tapirus*, were collected from Qinling Mountains. The exact locality of these fossils is on the hill slope behind the Donghe village, Luonan county, Shaanxi Province.

The human fossil tooth is larger than that of modern man, and also larger than the average size of Peking Man, but quite similar to those of Hexian Man, Yunxian Man and Java Man. It possesses the vertical furrows on both lingual and buccal surfaces. The shape of the crown is about rhomboid and has an obvious medial lingual angle. There are a couple of ridges on the slope of each cone. Judging from its morphology and size, Luonan tooth probably belongs to that of *Homo erectus*.

Except the size, the tooth of *Ailuropoda* is even less likely to be distinguished from those of common panda on its characteristics. The size of the tooth of Luonan *Ailuropoda* is much smaller than that of *A. melanoleus baconi*, distributing widely in the Middle and Late Pleistocene of southern China and larger than that of *A. microta*, a small type of Early Pleistocene, but rather similar to that of *A. m. fovealis* of late Early Pleistocene or modern panda. Owing to its deeper petrification and associated with primitive human fossil, the panda fossil of Luonan would rather belong to *A. m. fovealis* than modern one.

According to the fossil evidence and the stage of human evolution, the geological age of these fossils from Luonan may be early Middle Pleistocene or Late Early Pleistocene.

Fig. S8 Copy of English abstract of the paper describing found maxillary molar in Luonan Basin (1987, the original paper is in Chinese with English abstract)